Available online at www.sciencedirect.com
ScienceDirect
Journal of Power Sources 158 (2006) 1456–1462
JOURNAL OF POWER SOURCES
www.elsevier.com/locate/jpowsour

# Corrosion behavior of Pb–Sn and Pb–2 mass% Sn–Sr alloys during repetitive current application

Masami Taguchi [a,*], Tokiyoshi Hirasawa [b], Keiichi Wada [b]

[a] *Faculty of Engineering and Resource Science, Akita University, Akita 010-8502, Japan*
[b] *Advanced Battery Technology Laboratory, Shin-Kobe Electric Machinery Co. Ltd., Saitama 369-0297, Japan*

Received 30 August 2005; accepted 18 October 2005
Available online 15 December 2005

**Abstract**

Pb–Sn alloys of 0–2.0 mass% Sn and Pb–2 mass% Sn–Sr alloys of 0–0.50 mass% Sr were evaluated by the corrosion test with repetitive current application. The mass change of the specimen electrode depends on both the production of the corrosion scale and its peeling off. The oxygen generation on the alloy electrodes is also directly linked to the peeling off of the corrosion scale, resulting in the formation of corrosion powders in the electrolyte. For these Pb alloys, tin acts as an oxygen generation reducer and it may activate the production of the corrosion scale, which consists of $PbO_2$ and $PbSO_4$. Therefore, it seems that the increasing Sn content causes a decrease in the amount of the corrosion powder along with the growth of the corrosion scale. On the other hand, strontium has no influence on the corrosion resistance of the Pb–2 mass% Sn–Sr alloy unless the Sr content is 0.46 mass% or more. The change in the crystal structure from a coarser columnar to a fine granular may account for the deterioration of the corrosion resistance at the Sr content of 0.46 mass% or more.


*Keywords:* Lead-acid battery; Grid materials; Corrosion; Lead-tin alloys; Lead–tin–strontium alloys; Electrifying

## 1. Introduction

Since some lead-acid batteries are expected to be the power source for hybrid electric vehicles and other applications, consumers are requiring a marked improvement in its life time as well as capability [1–3]. The improvement of the life time may essentially depend on the grid materials [4]. The Pb–Sb alloys were first considered as grid materials, because this cycle performance is excellent under deep charge-discharge conditions. However, the Pb alloys have a shortcoming which does not pertain to maintenance-free batteries. That is to say, the dissolution of Sb into the electrolyte, which is followed by the subsequent deposition of metallic Sb on the negative electrode, leads to a higher water consumption of the electrolyte [5,6]. Next, the maintenance-free battery, which uses Pb–Ca–Sn alloys [7–11] as the grid materials to reduce the water consumption, were developed to increase its share in the auto industry. However, the grids of Pb–Ca–Sn alloys still have the following quality defects: (1) insufficient workability, (2) severe corrosion of the low Sn compositions and (3) insufficient life-time under deep charge-discharge conditions and at high temperature. On the other hand, the Pb–Sn–X alloys may be notable as the next grid materials, because the resistance of the Pb–Sn alloys to intergranular corrosion is relatively high in addition to its good workability. The above-mentioned X is the third content, which has improved some properties. For example, the addition of strontium to the Pb–Sn alloy has been reported to decrease the thickness of the corrosion scale [12] However, there has been only a little amount of information on the corrosion behavior of the Pb–Sn and Pb–Sn–X alloys during charge-discharge cycling, because the corrosive condition during use is complex. In this study, Pb–Sn alloys of 0–2.0 mass% Sn and Pb–2 mass% Sn–Sr alloys of 0–0.50 mass% Sr were examined using a corrosion test with repetitive current drains of 100 A $m^{-2}$, which is modeled on the situation of the grid during charge-discharge cycling [13,14], in order to elucidate the dependence of their compositions on the corrosion characteristics. Moreover, both the crystal structure and the rate of electric quantity consumed for the oxygen generation of the Pb alloys were examined in order to discuss the influence on the corrosion behavior.

* Corresponding author. Tel.: +86 18 889 2421; fax: +81 18 889 2421.
*E-mail address:* taguchi@ipc.akita-u.ac.jp (M. Taguchi).

0378-7753/$ – see front matter © 2005 Elsevier B.V. All rights reserved.
doi:10.1016/j.jpowsour.2005.10.079

## 2. Experimental

### 2.1. Specimens

The specimens are pure Pb, 4 types of Pb–Sn alloys (Sn content; 0.5–2.0 mass%) and 12 types of Pb–2 mass% Sn–Sr alloys (Sr content; 0.05–0.50 mass%). They were prepared from pure Pb (purity; 99.99 mass%), pure Sn (purity; 99.99 mass%) and the Pb–Sr alloy (Sr content; 1.50 mass%) by atmospheric casting. The weighed metal and alloy were melted in a graphite crucible at 773–823 K and then poured into an iron mold, which was preheated at 473 K. The rod-like ingots of 8 mm in diameter and 130 mm in length were cooled in air and the chemical compositions were analyzed using ICP spectroscopy(SEI, SPS4000). Table 1 shows the chemical composition of the specimens. Moreover, some specimens were polished on a series of abrasive papers and buffed with fine $Al_2O_3$ powders. After the chemical polishing with a mixed solution of acetic acid and hydrogen peroxide, the microstructures of the specimens were observed using a metallurgical microscope.

### 2.2. Corrosion test with repetitive current application

The specimen electrodes with a reaction area of 216.8 $mm^2$ were prepared from the rod-like ingots. They were washed in a supersonic bath containing ethanol and then evaluated by the corrosion test for 604.8 ks with repetitive current application in 4.50 kmol $m^{-3}$ $H_2SO_4$ at 348 K [14]. That is to say, a current density of 100 A $m^{-2}$ was applied to the specimen electrode for 21.6 ks and the immersion without any current drain for 21.6 ks were duplicated 14 times using a programmable DC power supply (ADVANTEST, R6145). The bath voltage between the specimen electrode and the counter Pt sheet was measured by an electrometer (ADVANTEST, R8240). After the corrosion test, the specimen electrode was washed with a distilled water and dried in a vacuum in order to weigh, and then the surface was analyzed by X-ray diffraction (JEOL, JDX-3530) to identify the corrosion products. The electrolyte was also filtered through a glass filter (IWAKI, 1G2). After weighing, the residue on the filter, which was suspended in the electrolyte during the corrosion test, was also analyzed by XRD.

Table 1
Chemical composition of specimens

| Sample | Sn (mass%) | Sr (mass%) |
|---|---|---|
| Pure Pb | – | – |
| Pb–0.5% Sn | 0.61 | – |
| Pb–1.0% Sn | 1.05 | – |
| Pb–1.5% Sn | 1.63 | – |
| Pb–2.0% Sn | 2.18 | – |
| Pb–2% Sn–0.05% Sr | 1.69 | 0.03 |
| Pb–2% Sn–0.10% Sr | 2.14 | 0.09 |
| Pb–2% Sn–0.15% Sr | 1.66 | 0.13 |
| Pb–2% Sn–0.20% Sr | 1.86 | 0.17 |
| Pb–2% Sn–0.23% Sr | 1.96 | 0.23 |
| Pb–2% Sn–0.25% Sr | 2.01 | 0.25 |
| Pb–2% Sn–0.30% Sr | 1.96 | 0.30 |
| Pb–2% Sn–0.32% Sr | 2.05 | 0.32 |
| Pb–2% Sn–0.35% Sr | 2.20 | 0.36 |
| Pb–2% Sn–0.40% Sr | 2.08 | 0.37 |
| Pb–2% Sn–0.45% Sr | 2.00 | 0.46 |
| Pb–2% Sn–0.50% Sr | 2.19 | 0.51 |

### 2.3. Measurement of oxygen generated from electrode

In order to evaluate the rate of electric quantity consumed for the oxygen generation, the specimen electrode with a reaction area of 28.3 $mm^2$ was prepared using an epoxy resin. While passing a current of 100 A $m^{-2}$ through the specimen electrode in 4.50 kmol $m^{-3}$ $H_2SO_4$ at 298 K, the oxygen generated from the electrode was collected in order to measure the volume using a microburet. Using Faraday's law, the rate of electric quantity consumed for the oxygen generation was calculated from the quantity of electricity passed through the specimen electrode and the volume of the generated oxygen.

## 3. Results

### 3.1. Microstructures of Pb–2 mass% Sn–Sr alloys

Fig. 1 shows the microstructures of the various Pb–2 mass% Sn–Sr alloys. The examination point is the middle between the surface and the center of the ingot. The Pb–2 mass% Sn–Sr alloys of 0–0.30 mass% Sr have a columnar structure, whose major axis is parallel to the direction of heat transfer during the casting (see Fig. 1(a)–(c)). However, the microstructure of the Pb–2 mass% Sn–Sr alloy abruptly changed to a fine granular crystal, in which the majority of the grains have a diameter of about 10 μm, when the Sr content is 0.46 mass% or more (see Fig. 1(d)).

Fig. 2 shows the relationship between the number of crystal grains per unit area and the Sn or Sr content for the Pb–Sn and Pb–2 mass% Sn–Sr alloys. The number of crystal grains near the surface is greater than those at the center or near the middle between the surface and the center. Therefore, the mean values for the three points were plotted with the number of crystal grains per unit area. Although the number of crystal grains of the Pb–Sn alloys increased with the increasing Sn content in the range of 0–1.05 mass%, the value decreased at 2.18 mass% Sn. These data show that the increasing Sn content does not necessarily lead to a grain refinement of the Pb–Sn alloys. On the other hand, the number of crystal grains in the Pb–2 mass% Sn–Sr alloys fluctuate from 7 to 26 grains $mm^{-2}$ in the range of 0–0.30 mass% Sr. However, the number of crystal grains dramatically increases to almost 9000 grains $mm^{-2}$ at 0.51 mass% Sr. This abrupt increase is caused by the preceding change in the micro structure from the columnar crystal to the fine granular one.

### 3.2. Corrosion behavior of Pb–2 mass% Sn–Sr alloys

Fig. 3 is an example of the change in bath voltage as a function of time during the corrosion test with repetitive cur-

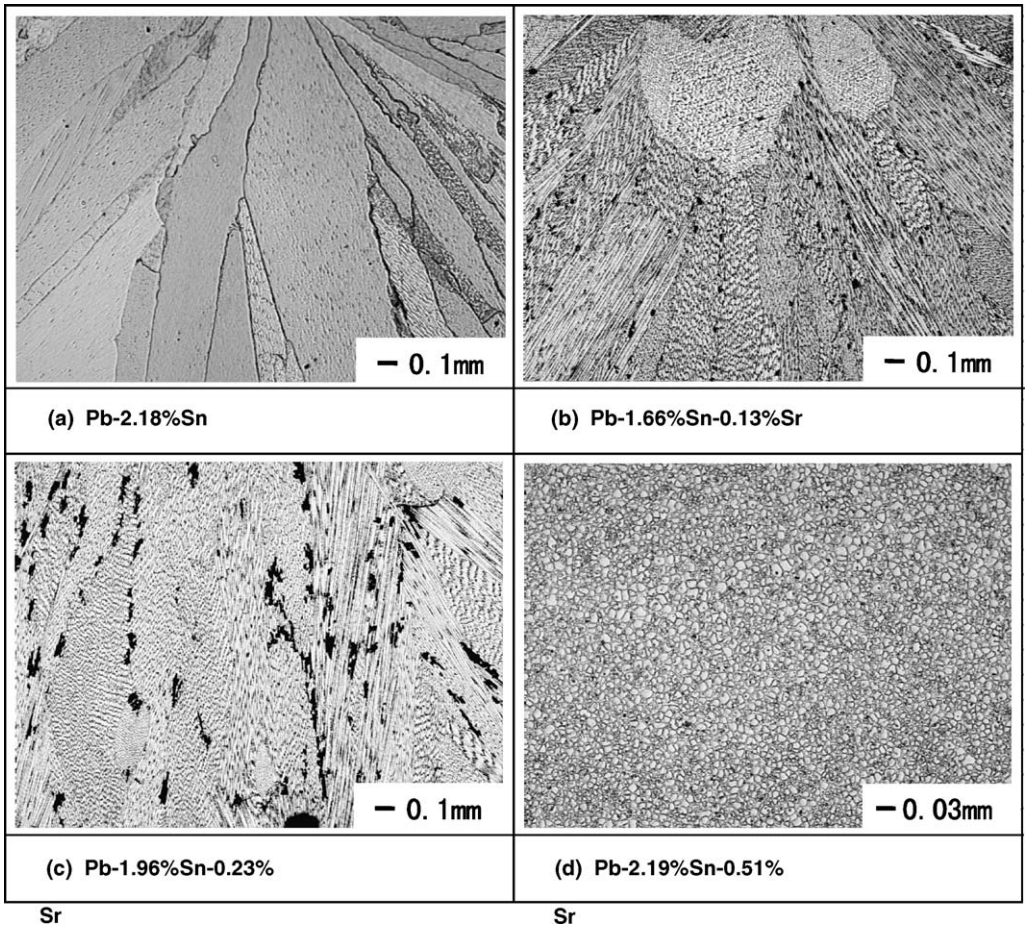


Fig. 1. Microstructures of various Pb–2 mass% Sn–Sr alloys.

rent application. For the Pb–2.18 mass% Sn and Pb–1.86 mass% Sn–0.17 mass% Sr alloys, both bath voltages at 100 A $m^{-2}$ were in the range from 2.1 to 2.2 V. To be exact, the bath voltage of the Pb–1.86 mass% Sn–0.17 mass% Sr alloy is slightly higher than that of the Pb–2.18 mass% Sn alloy. However, the difference in the bath voltages between the two Pb alloys becomes smaller as the number of cycles increases. When the test condition is switched from 100 A $m^{-2}$ to immersion without current appli-

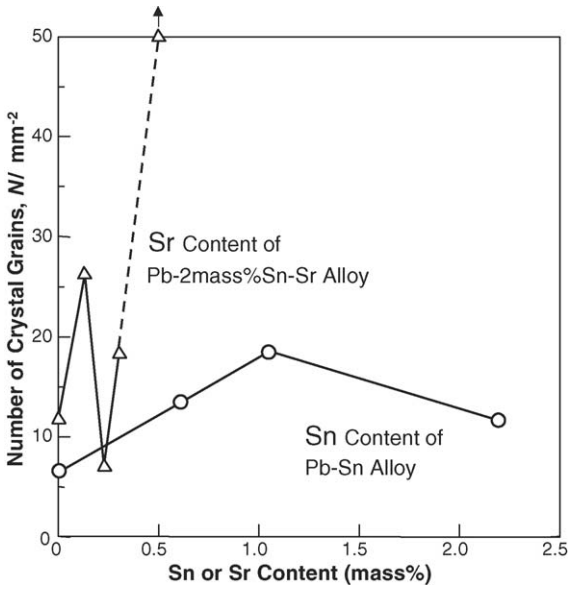


Fig. 2. Relationship between number of crystal grains and alloying contents for Pb–Sn and Pb–2 mass% Sn–Sr alloys.

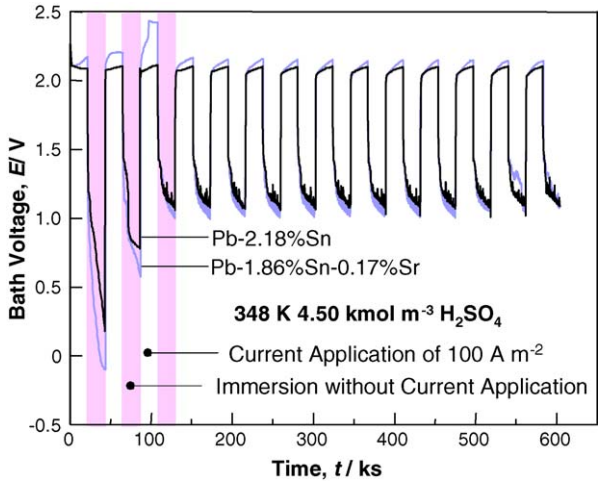


Fig. 3. Change in bath voltage as a function of time during corrosion test for Pb–2.18 mass% Sn and Pb–1.86 mass% Sn–0.17 mass% Sr alloys. A current applicationof 100 A $m^{-2}$ for 21.6 ks and immersion for 21.6 ks were repeated 14 times in 4.50 kmol $m^{-3}$ $H_2SO_4$ at 348 K.

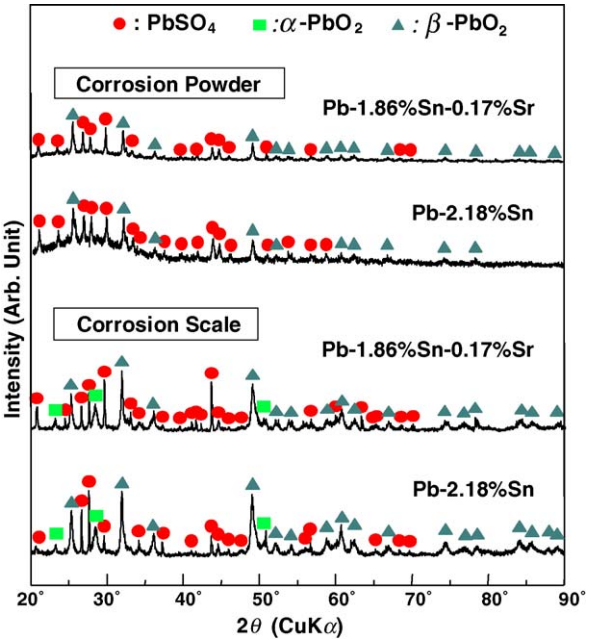


Fig. 4. XRD patterns of corrosion scales and corrosion powders for Pb–2.18 mass% Sn and Pb–1.86 mass% Sn–0.17 mass% Sr alloys.

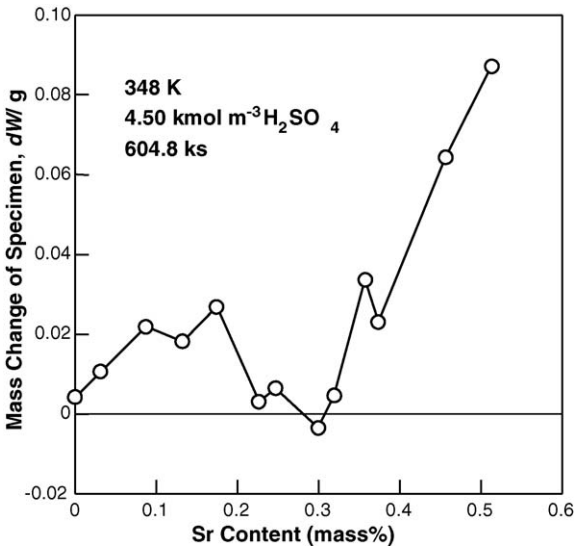


Fig. 5. Influence of Sr content on mass change of specimen during corrosion test for Pb–2 mass% Sn–Sr alloys.

cation, the bath voltage immediately falls to 1.3–1.4 V and then slowly decreases. The final voltage during immersion without current application becomes higher with cycling. The values are about 0 V in the first cycle, 0.6–0.8 V in the second cycle, and then they become fairly stable at 1.0–1.1 V when the cycle number is 3 or more. This phenomenon suggests that the corrosion scale on the specimen electrode becomes stable after 3 cycle or more.

The corrosion test with repetitive current application resulted in the formation of a dark brown corrosion scale on the specimen electrode. Fine black powders also deposited under the electrode and some of the powder became suspended in the electrolyte. These powders are called "corrosion powders" in this study. Fig. 4 shows the XRD patterns of the corrosion scales and the corrosion powders for the Pb–2.18 mass% Sn and Pb–1.86 mass% Sn–0.17 mass% Sr alloys. The corrosion scales produced on both the Pb alloys are recognized as a mixture of $PbSO_4$, α-$Pb_2$ and β-$PbO_2$. Although these three compounds were identified by XRD analysis for all the Pb–2 mass% Sr alloys, the intensity ratios of $PbSO_4$, α-$Pb_2$ and β-$PbO_2$ were not quite equal. On the other hand, the corrosion powders of the Pb–2.18 mass% Sn and Pb–1.86 mass% Sn–0.17 mass% Sr alloys are recognized as a mixture of $PbSO_4$ and β-$PbO_2$. Compared with the XRD patterns of the corrosion scales, there were no peaks from α-$Pb_2$. However, the cause of the disappearance is unknown at present.

Fig. 5 is the influence of the Sr content on the mass change of the specimen electrode during the corrosion test for the Pb–2 mass% Sn–Sr alloys. Correctly, the mass change is defined as the difference of the mass of the specimen electrode between before and after the corrosion test. There is a minute amount of mass gain for the Pb–2 mass% Sn alloy. For the Pb–2 mass% Sn–Sr alloys of 0.17 mass% Sr or lower, the mass of the specimen electrode increases with the increasing Sr content and its mass gain becomes about 0.02 g in the range of 0.09–0.17 mass% Sr. However, the mass change is depressed to be −0.004–0.007 g in the range of 0.23–0.32 mass% Sr. The mass change then increases again when the Sr content is greater than 0.35 mass%. In particular, the mass gains of the specimens of 0.46 and 0.51 mass% Sr are significant, which are several times greater than the mass gains of the other Pb–2 mass% Sn–Sr alloys. Fig. 6 shows the influence of the Sr content on the amount of corrosion powder for the Pb–2 mass% Sn–Sr alloys. For the Sr content of 0–0.13 mass%, the addition of Sr may be effective in suppressing the amount of the corrosion powder. However, the addition

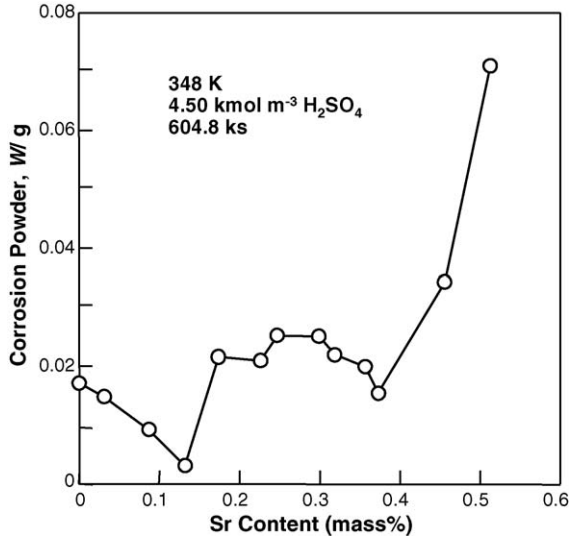


Fig. 6. Influence of Sr content on amount of corrosion powder in electrolyte during corrosion test for Pb–2 mass% Sn–Sr alloys.

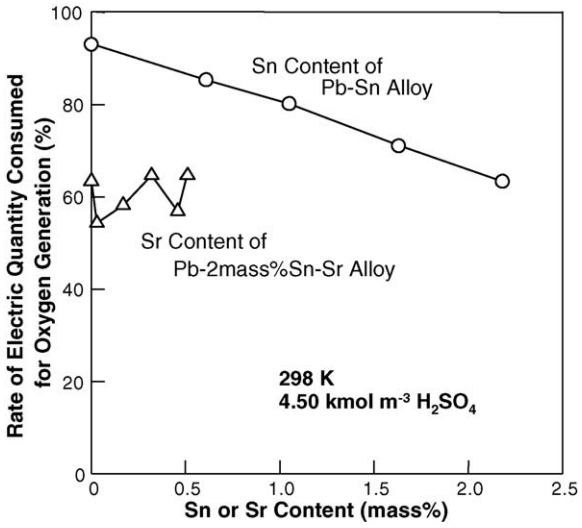


Fig. 7. Influence of Sn or Sr content on rate of electric quantity consumed for oxygen generation for Pb–Sn and Pb–2 mass% Sn–Sr alloys. The measurement of oxygen generated from electrode was carried out in 4.50 kmol $m^{-3}$ $H_2SO_4$ at 298 K.

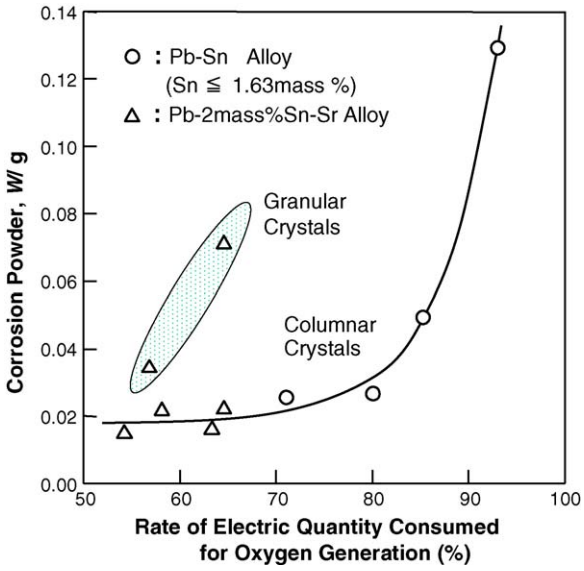


Fig. 8. Relationship between amount of corrosion powder produced in electrolyte during corrosion test and rate of electric quantity consumed for oxygen generation for Pb–Sn and Pb–2 mass% Sn–Sr alloys.

of 0.17–0.37 mass% Sr would result in a large amount of corrosion powder of about 0.02 g. Moreover, the amount of corrosion powder rapidly increases when the Sr content is 0.46 mass% or greater. When comparing Fig. 6 with Fig. 5, the mass gain of the specimen electrode maybe suppressed in the Sr content range in which the amount of the corrosion powder is high, and vice versa. Consequently, the decrease in the thickness of the corrosion scale does not always mean an improvement in the corrosion resistance of the Pb–2 mass% Sn–Sr alloys. In addition, the amount of corrosion powder as well as the mass gain are significant for the Pb–2 mass% Sn–Sr alloys of 0.46 mass% Sr or more, whose crystal structure must become a fine granular.

### *3.3. Rate of electric quantity consumed for oxygen generation for Pb–Sn and Pb–2 mass% Sn–Sr alloys*

Fig. 7 shows the influence of the Sn or Sr content on the rate of electric quantity consumed for the oxygen generation by the Pb–Sn and Pb–2 mass% Sn–Sr alloys. Since the magnitude of error depended on the convection of the electrolyte by unequal heating, the measurement temperature was set not at 348 K but at 298 K. In other words, the specimen electrode was electrolyzed at a current density of 100 A $m^{-2}$ for 10.8 ks in 4.50 kmol $m^{-3}$ $H_2SO_4$ at 298 K. The amount of oxygen generation was measured using a precise buret and then the rate of electric quantity consumed for the oxygen generation Eq. (1) [15,16] was calculated based on Faraday's law.

$$H_2O(1) \rightarrow 2H^+ + 1/2O_2 + 2e^- \quad (1)$$

The rate of electric quantity consumed for oxygen generation of pure Pb is the highest, which is 93% on average. The rate of the Pb–Sn alloys linearly depends upon the Sn content. That is to say, the rate of electric quantity consumed for the oxygen generation decreases with the increasing Sn content to be no more than 63% at 2.18 mass% Sn. On the other hand, the rate of electric quantity consumed for oxygen generation of the Pb–2 mass% Sn–Sr alloys is nearly independent on the Sr content, although it varies widely from 54 to 64% in the range of 0–0.51 mass% Sr.

## 4. Discussion

During current application at 100 A $m^{-2}$, the dissolution of the major constituent of the Pb alloy or Pb into the electrolyte probably occurs along with the oxygen generation as shown by Eq. (1).

$$Pb(alloy) \rightarrow Pb^{2+} + 2e^- \quad (2)$$

The $Pb^{2+}$ ions then react with $SO_4{}^{2-}$ ions to precipitate $PbSO_4$ on the surface of the Pb alloy [17,18]. A little of the precipitate also may suspend in the electrolyte immediately. In addition, a part of the $Pb^{2+}$ ions may be oxidized to $PbO_2$.

$$Pb^{2+} + SO_4{}^{2-} \rightarrow PbSO_4 \quad (3)$$

$$Pb^{2+} + 2H_2O \rightarrow PbO_2 + 4H^+ + 2e^- \quad (4)$$

Since the above-mentioned reactions need an electron conductor as the site for the electron transfer, the surface of the Pb alloy at the beginning of reaction and the surface of $PbO_2$ in contact with $PbSO_4$ shortly thereafter would perform this task.

Fig. 8 shows the relationship between the amount of the corrosion powder produced during the corrosion test and the rate of electric quantity consumed for the oxygen generation for the Pb–Sn and Pb–2 mass% Sn–Sr alloys. The amount of the corrosion powder for the Pb alloy with a high rate

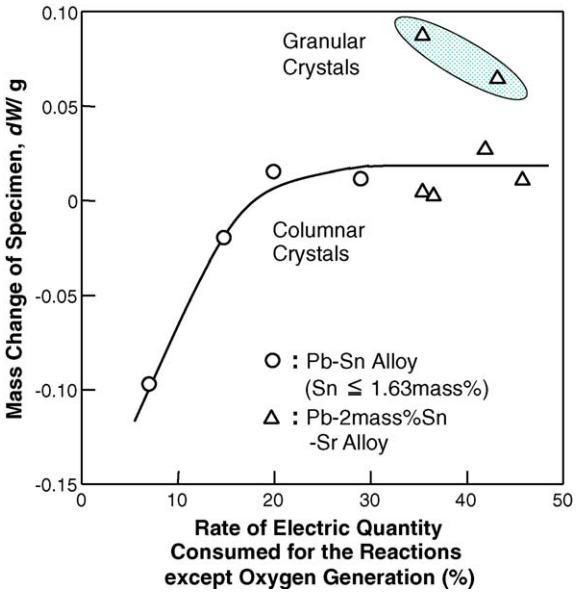


Fig. 9. Relationship between mass change of specimen during corrosion test and rate of electric quantity consumed for the reactions except oxygen generation for Pb–Sn and Pb–2 mass% Sn–Sr alloys.

of electric quantity consumed for the oxygen generation is greater than that for one with a low rate. Especially, when the rate is greater than 80%, the amount of the corrosion powder remarkably increases. The XRD analysis revealed that the corrosion powders were essentially the same as the corrosion scale on the specimen electrodes, which consisted with $PbSO_4$ and β-$PbO_2$ (see Fig. 4). These data strongly suggest that the scales are peeling off and become the corrosion powder, and the oxygen generation plays an important role in this peeling off. If the oxygen generation occurs at the boundary between the corrosion scale and the Pb alloy substrate, the significant force of the nascent oxygen would definitely promote the peeling of the corrosion scale. Incidentally previous studies [13,14] verified that the corrosion test of Pb-0.08 mass% Ca–Sn alloys without current application scarcely had any corrosion powder, even though the corrosion powder significantly occurred during the test with repetitive current application. It seems that this fact supports the preceding interpretation. On the other hand, the crystal structure of the substrate probably has an influence on the corrosion of the Pb–2 mass% Sn–Sr alloys. The amounts of the corrosion powder for the Pb–2 mass% Sn–Sr alloys with fine granular crystals are 2–3.5 time that for the alloy with columnar crystals. Therefore, it can be assumed that the form of the corrosion scale and its adhesion to the substrate depend on the crystal structure.

Fig. 9 is the relationship between the mass change of specimen electrode during corrosion test and the rate of electric quantity consumed for the reactions except for the oxygen generation of the Pb–Sn and Pb–2 mass% Sn–Sr alloys. For the Pb–Sn alloys of 1.63 mass% Sn or less, the mass change of the specimen significantly increases from −0.097 to about 0.02 g when the rate of electric quantity consumed for the reactions except for the oxygen generation increases from 7 to 29%. The mass change from minus to plus can be explained by the decrease in the amount of the corrosion powder, which is shown in Fig. 8. The Sn in the Pb alloy serves to suppress the oxygen generation of Eq. (1) and activate the other reactions of Eq. (2)–(4), namely, the production of $PbSO_4$ and $PbO_2$. What is most important maybe that the suppression of the oxygen generation leads to an improved resistance to the peeling off of the corrosion scale, resulting in a decreased amount of the corrosion powder. Moreover, the influence of the crystal structure on the mass change of the Pb–2 mass% Sn–Sr alloys can be interpreted by the same one as the corrosion powder. The mass change of the Pb–2 mass% Sn–Sr alloys with columnar crystals is constant at around 0.02 g, without regard to the Sr content. However, the large Sr content of 0.46 or 0.51 mass% may cause a decrease in the corrosion resistance of the Pb–2 mass% Sn–Sr alloys, which is related to the change in the micro structure from columnar to fine granular.

## 5. Conclusions

The mass changes in the Pb–Sn and Pb–2 mass% Sn–Sr alloys during the corrosion test with the repetitive current application depend on the production of the corrosion scale and its peeling off. The peeling off of the scale, which is significantly related to the production of the corrosion powder, also may be caused by the oxygen generation on the Pb alloy surface. For these Pb alloys, the alloying of Sn with Pb suppress the oxygen generation, and in addition, it probably activates the production of $PbSO_4$ and $PbO_2$. Therefore, the increasing Sn content leads to a significant decrease of the corrosion powder in the electrolyte and the growth of a corrosion scale on the Pb alloy surface. On the other hand, the Sr content may have no influence on the corrosion resistance of the Pb–2 mass% Sn–Sr alloys unless the Sr content is 0.46 mass% or more. However, it can be concluded that the crystal structure change for the high Sr contents, which is from a coarser columnar to a fine granular having the grain size of about 1.0 μm in diameter, significantly reduces the corrosion resistance.

## References

[1] M. Taguchi, K. Fukui, J. Japan Inst. Metals 68 (2004) 887.
[2] M. Taguchi, H. Sugita, J. Power Sources 109 (2002) 294.
[3] T. Takamura, Electrochemistry 68 (2000) 615.
[4] M. Otsuka, FB Technical News 59 (2003) 1.
[5] T. Hirasawa, K. Sasaki, M. Taguchi, K. Kaneko, J. Power Sources 85 (2000) 44.
[6] T. Laitinen, K. Salmi, G. Sundholm, B. Monahov, D. Pavlov, Electrochim. Acta 36 (1991) 605.
[7] H. Giess, J. Power Sources 53 (1995) 31.
[8] R. Miraglio, L. Albert, A. El Ghachcham, J. Steinmetz, J.P. Hilger, J. Power Sources 53 (1995) 53.
[9] C.S. Lakshimi, J.E. Manders, D.M. Rice, J. Power Sources 73 (1998) 23.
[10] H. Tsubakino, M. Tagami, S. Ioku, A. Yamamoto, Meta. Mater. Trans. 27A (1996) 1675.
[11] A. Komaki, S. Saito, S. Matsubayashi, Z. Takehara, Denki Kagaku 64 (1996) 47.
[12] T. Hirasawa, K. Wada, Unpublished data.
[13] M. Taguchi, T. Hirasawa, Mate. Trans. JIM 41 (2000) 1307.

[14] M. Taguchi, Y. Hiramatsu, T. Hirasawa, N. Tanaka, J. Japan Inst. Metals 65 (2001) 720.
[15] A.J. Bard, R. Parsons, J. Jordan:, Standard Potentials in Aqueous Solution, Marcel-Dekker, 1985, pp. 49.
[16] W.M. Latimer:, Oxidation Potentials, Prentice-Hall, 1952, pp. 38–50.
[17] Y. Matsuda, Z. Takehara:, DenchiBinran, Maruzen, 2001, pp. 151.
[18] M. Taguchi, H. Sugita, J. Japan Inst. Metals 66 (2002) 670.